Orientation, Flow, and Clogging in a Two-Dimensional Hopper: Ellipses vs. Disks

Junyao Tang[1,2] and R. P. Behringer[1]

[1] *Department of Physics & Center for Nonlinear and Complex Systems, Duke University, Durham, NC, 27708, USA*

[2] *10451 Clay Road, TGS-Nopec Geophysical Co., Houston, TX, 77043, USA*

PACS 47.57.Gc – Granular flow
PACS 81.05.Rm – Porous materials; granular materials
PACS 78.20.Fm – Birefringence

Abstract –Two-dimensional (2D) hopper flow of disks has been extensively studied. Here, we investigate hopper flow of ellipses with aspect ratio $\alpha = 2$, and we contrast that behavior to the flow of disks. We use a quasi-2D hopper containing photoelastic particles to obtain stress/force information. We simultaneously measure the particle motion and stress. We determine several properties, including discharge rates, jamming probabilities, and the number of particles in clogging arches. For both particle types, the size of the opening, D, relative to the size of particles, ℓ is an important dimensionless measure. The orientation of the ellipses plays an important role in flow rheology and clogging. The alignment of contacting ellipses enhances the probability of forming stable arches. This study offers insight for applications involving the flow of granular materials consisting of ellipsoidal shapes, and possibly other non-spherical shapes.

Hopper flows of granular materials involve dynamical granular states with important industrial applications [1, 2]. Time-averaged granular flow theories, often using hopper flow as a test case, have progressed from continuum mechanics models to mesoscopic models [2–6]. Fluctuations and clogging (or jamming) are also important characteristics for hopper flow. Experiments [7–9] have examined the the clogging transition of hopper flow for different grain properties and hopper geometries. Most recent results from [8] imply that all hoppers have a nonzero probability to clog. Other studies [10–15] have also sought to understand flow and clogging (or jamming) mechanisms from a microscopic viewpoint. However, for simplicity, theories developed from the above studies often tend to assume spherical particles, including disks in two dimensions (2D). The effect of particle shape on hopper flow is usually not their focus. In reality, particle shapes are often not spherical; rice and M&M's are roughly ellipsoids; sand particles have irregular shapes. Thus, it is scientifically and industrially relevant to explore how particle shape affects flow rheology and clogging mechanisms.

A simple way to explore particle shape effects is to contrast 2D hopper flows of disks and ellipses for the time-averaged discharge rate, $\dot{M}$, and jamming probability. Discharge rates of hopper flow often follow the well-established Beverloo equation [16], which relates $\dot{M}$ to the hopper opening size, D : $\dot{M} \propto (D - kd_{avg})^{(n-1/2)}$, where n is the spatial dimension (e.g. $n = 2$ or 3 for two or three-dimensional systems). D is reduced by kd_{avg} due to boundary effects, where d_{avg} characterizes the grain size, and k is an order-one constant [2]. Recent studies [17, 18] have provided micromechanical insights into this equation with a coarse-grain technique. An important open question concerns the relevance of this relation for non-spherical particles. Several studies have used DEM simulation methods to understand how the aspect ratio of an ellipse could affect the discharge rate [21–27]. Their results are not consistent due to different assumptions such as particle shapes, frictional properties of particles and etc. A recent study by Liu et al. [28] utilizing both DEM and experiments, suggests a modified Beverloo equation for ellipse flow. They also show observations of flow characteristics based on their simulation results. To our knowledge, experimental investigations of hopper flow of ellipses based on particle-levels dynamics are still lacking.

In this paper we experimentally test the applicability

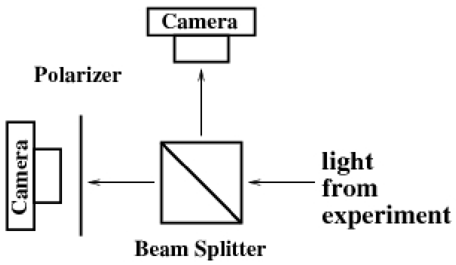

Fig. 1: Sketch of the synchronized camera set up. Light emerging from the hopper is split and imaged by two synchronized high-speed cameras, one with and the other without a crossed polarizer.

of the Beverloo equation to elliptical particles in quasi-2D hopper flows. We also measure the probablity of jamming for these particles. We contrast these quantities to results for bi-disperse disks in the same hopper. To apply the Beverloo equation, an issue arises for elongated particles such as ellipses: since there are two lengths for the particles, the major and minor principal axis lengths, d_{maj} and d_{min} respectively, which if either is relevant? Thus, there are two dimensionless length ratios, which can be taken as D/d_{min} and the ellipse aspect ratio, $\alpha = d_{maj}/d_{min}$. In addition, the organization of elliptical grains, and the stable structures that they form when a jammed state occurs following a clog are important.

In the present experiments, we use a 2D wedge-shaped hopper, as in our previous studies [10, 19]. The apparatus consists of two transparent Plexiglas sheets separated by aluminum spacers and aluminum hopper walls. The system is divided into upper and lower regions, both of which are hoppers. Approximately 5,000 bi-disperse circular particles or 3,000 identical elliptical particles are initially placed in the upper hopper section. For ellipses, d_{maj} = 10 mm, and d_{min} = 5 mm. For disks, we have big particles (diameter d = 6 mm) and small particles (diameter d = 5 mm) with relative fraction small to large of 2:1. So the average diameter of the bi-disperse circular particles (disks) is 5.3 mm. Two sliding Teflon bars initiate or stop the flow. The upper hopper can be reloaded easily by rotating twice about a pivot. Here, we consider results for a hopper wall angle θ_w=30^o (θ_w is half the full opening angle of the hopper). The particles are made of photoelastic materials (Vishay, PSM); when they are placed between crossed polarizers, transmitted light produces images with fringe-like patterns that depend on the forces acting on each particle [20]. We use the photoelastic response to measure grain-scale forces. The square of the image intensity gradient provides a measure of the local force, which we calibrate by applying known static loads to systems of particles [30]. Note that the contact forces between particles can also be accurately calculated based on photoelastic principles, for high-resolution images [31]. This is not possible in the present experiments that rely on high speed images with modest frame sizes.

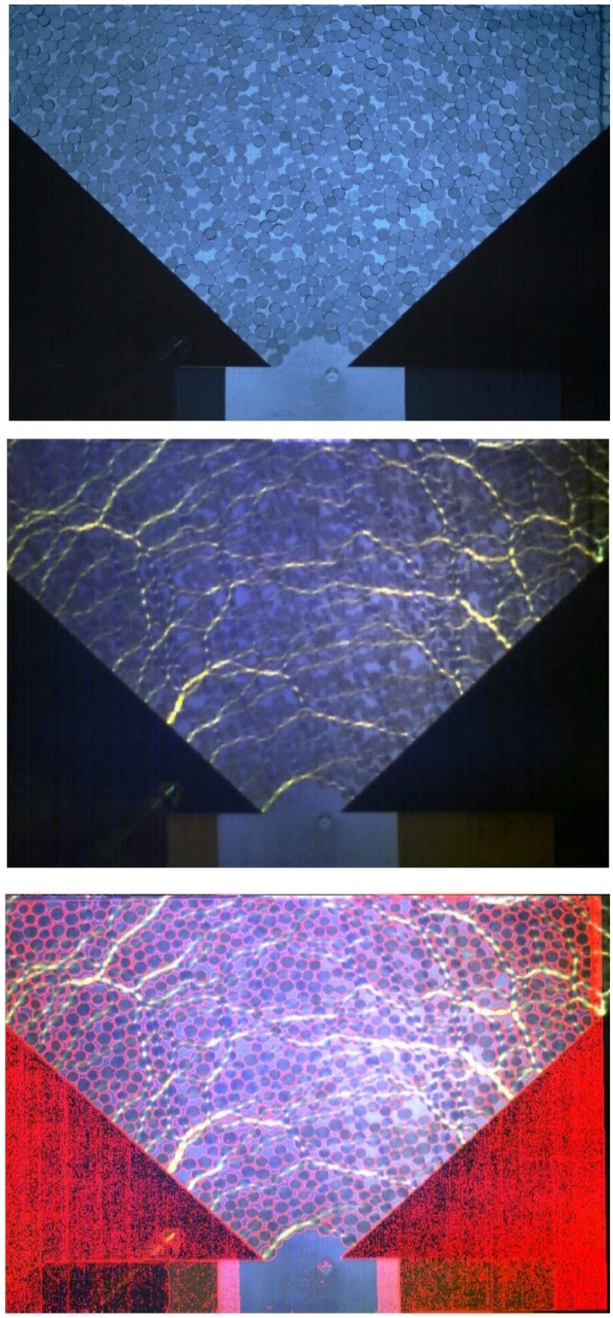

Fig. 2: (Color Online). Sample images from the top cameras, and their overlap. Top: A direct image. Middle: The corresponding polarized image. Bottom: The image that results from overlapping the top and middle images.

In order to simultaneously observe particles positions and the forces acting on them, we use two synchronized high-speed cameras (frame rate: 500fps), one to take pictures for particle tracking (Fig. 2-top) and the other for photoelastic measurements (Fig. 2-middle). As in Fig. 1, a beam splitter steers polarized light from the experiment into the two cameras. One camera has a polarizer that is crossed with respect to the original light polarization. The other lacks a second polarizer, and only registers the direct images of the particles. The images from the cameras are aligned through registration techniques to produce a composite image that details the location and orientation of particles, and the photoelastic response. Note that photoelastic images alone cannot be used to locate particles, since particles and/or their boundaries are often invisible. Fig. 2 shows two original (direct and polarized) images from the two cameras, and the resulting overlapped image. This figure shows the force chains corresponding to strongly stressed particles. Below, we use this dual information to understand key differences between the flow and clogging of ellipses vs. disks.

We start by comparing the time-averaged discharge rate for disks and ellipses. We measured $\dot{M}$ as the ratio of the total number of particles to the total time taken to empty the hopper. If a jam occurred, we re-initiated the flow by controlled taps with a small hammer located outside the Plexiglas. The total time to empty the material is the sum of the consecutive times during which the particles flowed. In Fig. 3, we show the discharge rate raised to the 2/3 power, $\dot{M}^{2/3}$, vs. the opening size, D. If the Beverloo equation holds, there should be a linear relation (in 2D) for $\dot{M}^{2/3}$ vs. D [16]. The data for both disks and ellipses are consistent with such a relation, $\dot{M}^{2/3} = SD + C$, and hence the Beverloo equation is satisfied (The fitting parameters S and C appear in Fig. 3 and Fig. 4). In physical units, the ellipses flow more slowly than the disks at the same opening size; $\dot{M}$ data in Fig. 3 for the ellipses have a slope that is close to 1/2 that for the disks. Where might such a difference arise? Also, what is a reasonable way to compare these two data sets, given that the minor axis of the ellipses is comparable to the diameter of the disks, but the major axis is roughly twice the disk diameter? The Beverloo equation does not provide insight (except in a rough way through the boundary layer term, gkd_{avg}) into the role of particle shape.

One approach is to seek non-dimensional rescaled representations of the data for $\dot{M}$ and D. The former, has dimensions of inverse time. The time scale must come from g and a length scale related to the particle size. Similarly, the scale for D involves a particle-scale length. For simplicity, we assume that the same measure, ℓ_i, which depends on the particle species ($i = d$ for disks or $i = e$ for ellipses) applies for both $\dot{M}$ and D. We write $\dot{M} = (g/\ell_i)^{1/2}\dot{M}'$ and $D = \ell_i D'$, where the primed quantities are dimensionless. Since $\dot{M}^{2/3} \propto D$, for dimensionless quantities: $\dot{M}'^{2/3} = (\ell_i/g)^{1/3}\dot{M}^{2/3} \propto \ell_i^{1/3}\ell_i D'$. There is a universal expression $\dot{M}'^{2/3} = S'D' + C'$ if $\ell_e^{4/3}S_e/\ell_d^{4/3}S_d = 1$. The measured slopes for ellipses and disks satisfy $S_d/S_e \simeq 2$, which yields $\ell_e^{4/3}/\ell_d^{4/3} \simeq 2$ This is roughly satisfied if $\ell_d = d$ and $\ell_e \simeq d_{maj}$. Then, $\ell_e^{4/3}/\ell_d^{4/3} = (d_{maj}/d)^{4/3} = 2.3$. This is reasonably consistent with the ratio of the slopes in Fig. 3, $S_d/S_e = 2.0\pm0.2$.

Fig. 4 shows data for the dimensionless flow rate $\dot{M}'$ vs. dimensionless hopper opening, D', for $\ell_e = 1.0$ cm $= d_{maj}$ as the length scale factor, and a best fit $\ell_e = 0.88$ cm. For the latter choice of ℓ_e, the collapse of the disk and ellipse flow rate data is complete, within the scatter.

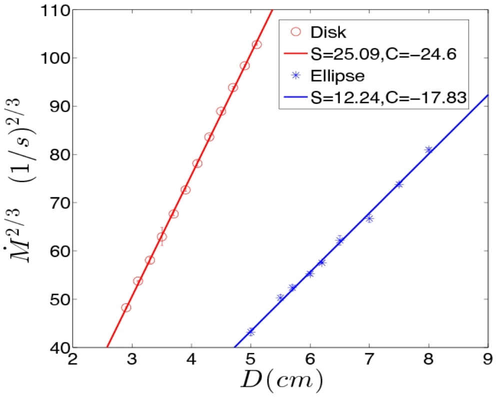

Fig. 3: (Color Online). Discharge rate vs opening sizes of disks and ellipses. (Hopper wall angle $\theta_w = 30^o$).

Previously [19], we showed for our disks that flowing/clogging can be described as a Poisson process. If the probability of flow without a clog in time dt is dt/τ_c, then the probability that the flow persists without clogging until time t is $P = \exp(-t/\tau_c)$, where the survival time τ_c reflects the the jamming probability of hopper flow. In Fig. 5, we compare the jamming probability of a system of disks and a system of ellipses, where, we use $\tau_c\dot{M}$ (at a given D), i.e., the average number of particles that fall out before jamming, similar to the term "n" used in [14]. For both particle types, $\tau_c\dot{M}$ grows strongly with D, consistent with exponential dependence, i.e., $ln(\tau_c\dot{M}) = AD + B$. Although the experimentally accessible ranges of D for the two data types do not overlap, extrapolation suggests that ellipse flows jam more readily than disk flows at the same D. Like the flow rate, it is interesting to rescale the physical quantities in Fig. 5. The vertical axis is already dimensionless. If we rescale D by the mean diameter of the disks and by the major diameter of the ellipses, we obtain a good collapse of the disk and ellipse data for $\tau_c\dot{M}$, as shown in Fig. 6 ($ln(\tau_c\dot{M}) = A'D' + B'$), where the primes here refer to fits to the scaled dimensionless data.

As discussed previously [11, 12, 20], the formation of transient force chains during hopper flow is related to the stick-slip events of hopper flow, which in turn control the flow rate and rheology. Hence, we expect that a larger probability of forming long-lived force chains (e.g. near the opening) will be correlated with a lower discharge rate.

In the random-walk model of To et al. [13,14], the probability of stable blocking arches near the opening depends largely on the number of particles in the arch. If we assume that D relative to particle size is the only relevant factor, we might argue that for the same hopper opening size, the hopper flow of ellipses needs fewer particles to form the blocking arch than the hopper flow of disks, since for $\dot{M}$, the microscopic length scale for the ellipses is double that for disks. Alternatively, if a flow of ellipses where the

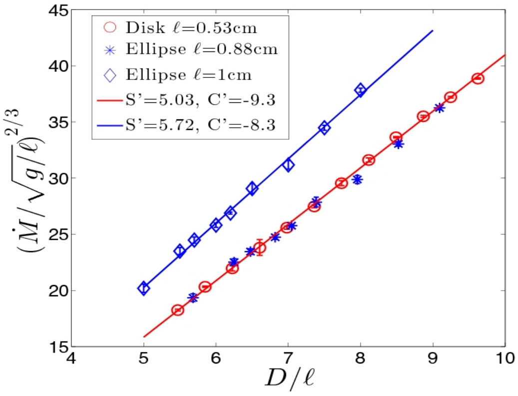

Fig. 4: (Color Online). Dimensionless discharge rate vs. dimensionless opening size for disks and ellipses. (Hopper wall angle $\theta_w = 30^o$).

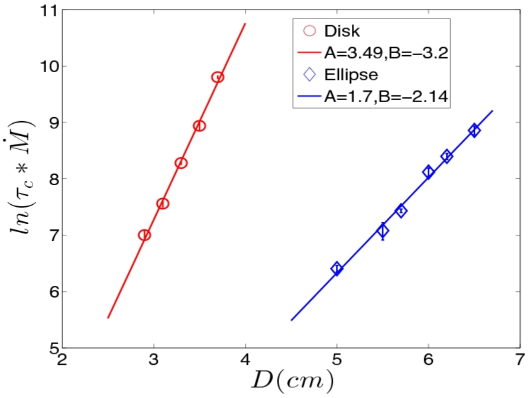

Fig. 5: (Color Online). Semi-log plot of $\tau_c \dot{M}$ vs opening size for both disks and ellipses (hopper wall angle $\theta_w = 30^o$).

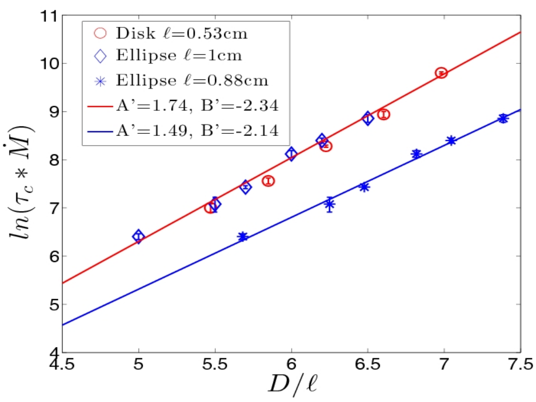

Fig. 6: (Color Online). Semi-log plot of $\tau_c \dot{M}$ vs opening size for both disks and ellipses (hopper wall angle $\theta_w = 30^o$). Dimensionless version. Stars correspond to the dimensionless data with the length scale $\ell_e = 0.88$ cm that collapse disks and ellipses discharge rate data in Fig 3.

opening size D_1 has the same clogging probability as a flow of disks where the opening is D_2, one might expect that there should be similar number of particles in the blocking arches for ellipses than for disks. However, this is not the case. Fig. 7 shows statistics for the number of particles in blocking arches for disks and ellipses, where the D's were chosen (differently) so that the two systems have similar jamming probabilities ($\tau_c \dot{M}$=1097 for disks and 1186 for ellipses, D=2.9cm for disks and 5.5cm for ellipses). Fig. 7 shows that for the ellipses, the number of particles forming the blocking arch has a wider distribution and sometimes can be as large as 18 particles. On average, the blocking arch consists of more particles for ellipses than for disks: 12 ellipses and 8 disks. Hence particle size is not the only differentiating factor between ellipse flow and disk flow.

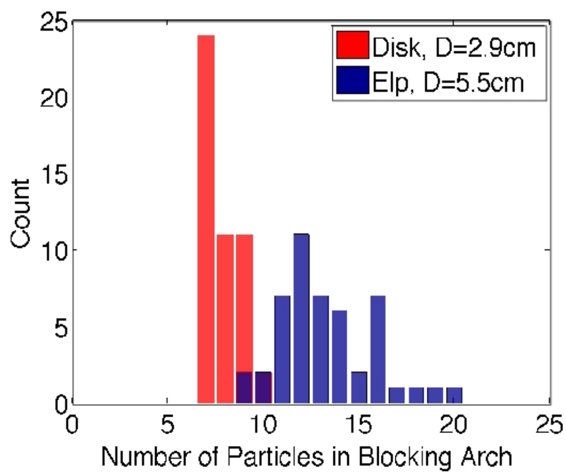

Fig. 7: (Color Online). Histogram of number of particles in the blocking arch for disks and ellipses.

Where does the additional effective stability for ellipses compared to disks come from? We address this question using synchronized particle tracking and photoelastic stress measurements.

The source of the difference lies in the fact that ellipses have a coupling between their orientation that affects their mechanical stability and local density. Successive frames from the synchronized videos of ellipses, e.g. Fig. 8, (a complete video is available at: [32]), show that ellipse rotation during the flow affects the force chain structure and stability. This rotation is not simply random.

Specifically, we find a systematic correlation between particle orientation and force chain orientation, defined below. Force chains tend to lie along lines corresponding to the local major principal stress. Using image registration and photoelastic techniques, we determine this direction by connecting lines through the centers of the ellipses that experience strong forces. We determine the mean force acting on a particle from the gradient-squared measure discussed above and in previous papers [29,30]. We characterize the orientations of contacting ellipses relative to their contact line, using the angles (θ_1, θ_2) illustrated in Fig. 9. Since (θ_1, θ_2) and (θ_2, θ_1) correspond to similar cases, we define $\theta_1 < \theta_2$. We collect all angle pairs for force

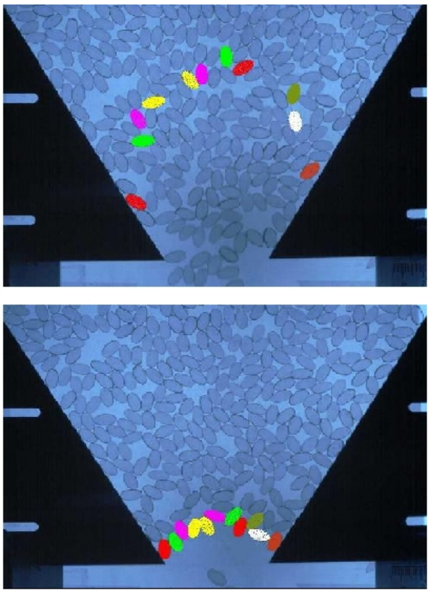

Fig. 8: (Color Online). Particle-tracking image analysis of sequence of a high speed video images showing how apparently random particles (brightly colored particles) form the arch that stops the flow. Note that a majority of the contacting neighbors for the blocking arch of ellipses tend to align roughly parallel.

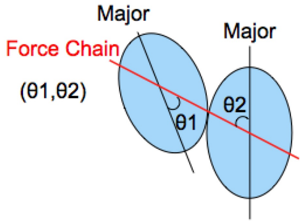

Fig. 9: (Color Online). Illustration of the angles (θ_1, θ_2) that characterize the orientations of contacting ellipses.

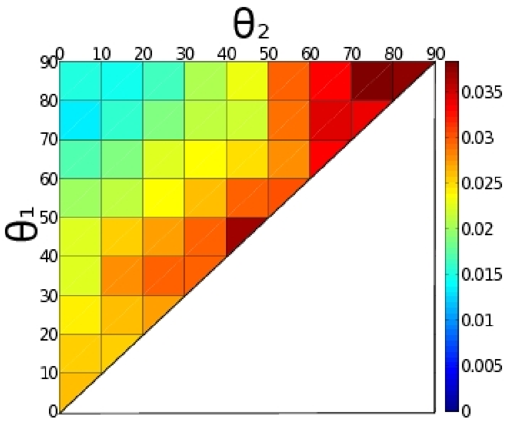

Fig. 10: (Color Online). 2D histogram of the probability distribution of (θ_1, θ_2) for stressed ellipses during flow.

chain particles (defined to be at or above the mean force) from approximately 1000 image sequences during a flow, and plot the resulting probability distribution in Fig. 10. There is a clear orientation preference: ellipses forming force chains tend to align parallel to their neighbors, with their directions normal to the contact line (i.e. the local direction of the force chain).

This parallel preference is even stronger if we limit the analysis to the force chains that jam the hopper at the outlet. These chains are usually among the strongest. They form a much smaller data set, but we show results below for about 100 cases. Fig. 11(a) shows the corresponding (θ_1, θ_2) probability distribution, and Fig. 11(b) shows the distribution along the line $\theta_1 = \theta_2$. There is clearly a strong preference for parallel alignment for neighboring particles in the jamming force chains.

This preferred orientation in strong force chains is a natural consequence of stability. Two neighboring particles differing significantly from this orientation, will typically rotate to a more stable, denser configuration where they are more parallel [33]. Simple stability analysis shows that approximate lines of particles with a parallel configuration can be stable, even without surrounding particles. These calculations are supported by a simple test: when multiple ellipses (we have tried up to 10 particles) are placed on a smooth surface in a parallel configuration, it is possible to compress the line of particles without buckling. Such configurations are hypostatic and a similar test with disks shows that even a very small number of particles in a line will buckle under uni-axial compression. This suggests a starting point for a more detailed quantitative approach to describing the relation between force networks and ellipse orientation. More experimental data, such as photoelastic measurements of ellipses with other aspect ratios, will be helpful for building theoretical models.

In this paper, we investigated the effect of particle shape on hopper flow by comparing flow properties of ellipses to those of disks. By comparing the discharge rate and jamming probability of ellipses to disks, we find that simple scaling laws allow us to map the flow rates and jamming probabilities of our elliptical particles onto those for disks. For both of these properties, the relevant particle length scale is close to the major diameter of the ellipses. Analysis of the synchronized particle-tracking and stress data shows that the strongly stressed elliptical particles that form the strong force chains, tend to align parallel to their neighbors and transverse to the direction of the force chains. This effect produces more stable force chains.

Acknowledgements: This work was supported by IFPRI and by NSF grant DMR-1206351.

REFERENCES

[1] Zuriguel I. *et al.*, *Scientific Reports*, **4** (2014) 7324.
[2] Nedderman R. M., *Statics and Kinematics of Granular Materials* (Cambridge University Press, Cambridge)) 1992.

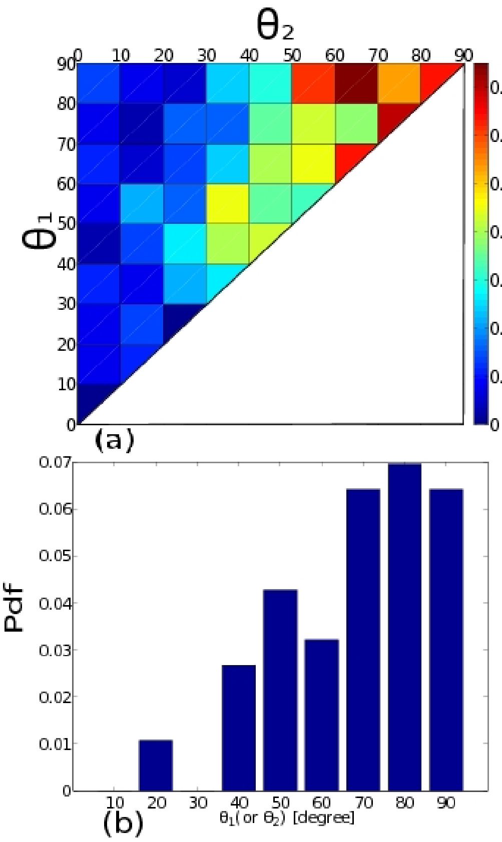

Fig. 11: (Color Online). (a): 2D histogram of the probability distribution of (θ_1, θ_2) for the jammed arch. (b): Quantitative plot of the histogram along the diagonal line of (a).

[3] K. K. Rao and P. R. Nott, *An Introduction to Granular Flow* (Cambridge Series in Chemical Engineering)) 2008.

[4] Kamrin K. and Bazant, M. Z., *Phys. Rev. E*, **75** (2007) 041301.

[5] Kamrin K. and Koval G., *Phys. Rev. Lett*, **108** (2012) 178301.

[6] G. D. R. Midi, *Euro. Phys. J. E.*, **14** (2004) 341.

[7] Zuriguel I., Garcimart A., Maza D., Pugnaloni L. A and Pastor J. M. , *Phys. Rev. E.*, **71** (2005) 051303.

[8] Thomas C. C. and Durian D. J., *Phys. Rev. Lett.*, **114** (2015) 1780011.

[9] Thomas C. C. and Durian D. J., *Phys. Rev. E.*, **87** (2013) 052201.

[10] Mort P., Michaels J. N., Behringer R. P., Campbelle C. S., Kondicf L., Kheiripour Langroudig M., Shattuckh M., Tang J., Tardosj G. I., and Wassgrenk C., *Powder Technology*, **284** (2015) 571.

[11] Gardel E., Sitaridou E., Facto K., Keene E., Hattam K., Easwar N. and Menon N., *Phil.Trans.R.Soc.*, **367** (2009) 5109.

[12] Ferguson A. and Chakraborty B., *Phys. Rev. E.*, **73** (2006) 011303.

[13] To K., *Phys. Rev. E.*, **71** (2005) 060301.

[14] To K. and Lai P. Y., *Phys. Rev. E.*, **66** (2002) 011308.

[15] Vivanco F., Rica S., and Melo F., *Granular Matter*, **14** (2012) 563.

[16] Beverloo W. A., Leniger H. A. and Van de Velde J., *Chem. Eng. Sci.*, **15** 260 (1961)

[17] Janda A., Zuriguel I., and Maza D., *Phys. Rev. Lett.*, **108** (2012) 248001.

[18] Rubio-Largo S. M., Janda A., Maza D., Zuriguel I. and Hidalgo R. C., *Phys. Rev. Lett.*, **114** (2015) 238002.

[19] Tang J. and Behringer R. P., *Proceedings of The 6th International Conference on Micromechanics of Granular Media*, **1145** (2009) 515.

[20] Tang J. and Behringer R. P., *Chaos*, **21** (2011) 041107.

[21] Cleary P. W., *Second International Conference on CFD in the Minerals and Process Industries*, **1** (1999) 71.

[22] Cleary P. W. and Sawle M. L., *Appl. Math. Models*, **26** (2002) 89.

[23] Tao H., Jin B. and Zhong W., *International Conference on Electric Technology and Civil Engineering (ICETCE)*, **1** (2011) 678.

[24] Langston P. A., Al-Awamleh M. A., Fraige F. Y., and Asmar B. N., *Chem. Eng. Sci.*, **59** (2004) 425.

[25] Li J. T., Langston P. A., Webba C. and Dyakowskia D., *Chem. Eng. Sci.*, **59** (2004) 5917.

[26] Cambell C. S., *Powder and Grains*, **2009** (2009) 591.

[27] Hhner D., Wirtz S. and Scherer V., *Powder Technology*, **235** (2013) 614.

[28] Liu S. D., Zhou Z. Y. and Yu A. B., *Powder Technology*, **253** (2014) 70.

[29] Ren J., Dijksman J. A. and Behringer R. P., *Phys. Rev. Lett.*, **110** (2013) 018302.

[30] Howell D. and Behringer R. P., *Phys. Rev. Lett.*, **82** (1999) 5241.

[31] Majmudar T. S. and Behringer R. P., *Nature*, **435** (2005) 1079.

[32] Tang J., *www.youtube.com/watch?v=p3lwWfF2dTI*, (2012) .

[33] Farhadi S., Zhu A. and Behringer R. P., *Phys. Rev. Lett.*, (2015–to appear)